Designing Nanoparticles and Nanoalloys with Controlled Surface and Reactivity

Sophie Carenco

Designing Nanoparticles and Nanoalloys with Controlled Surface and Reactivity

Sophie Carenco*[a]

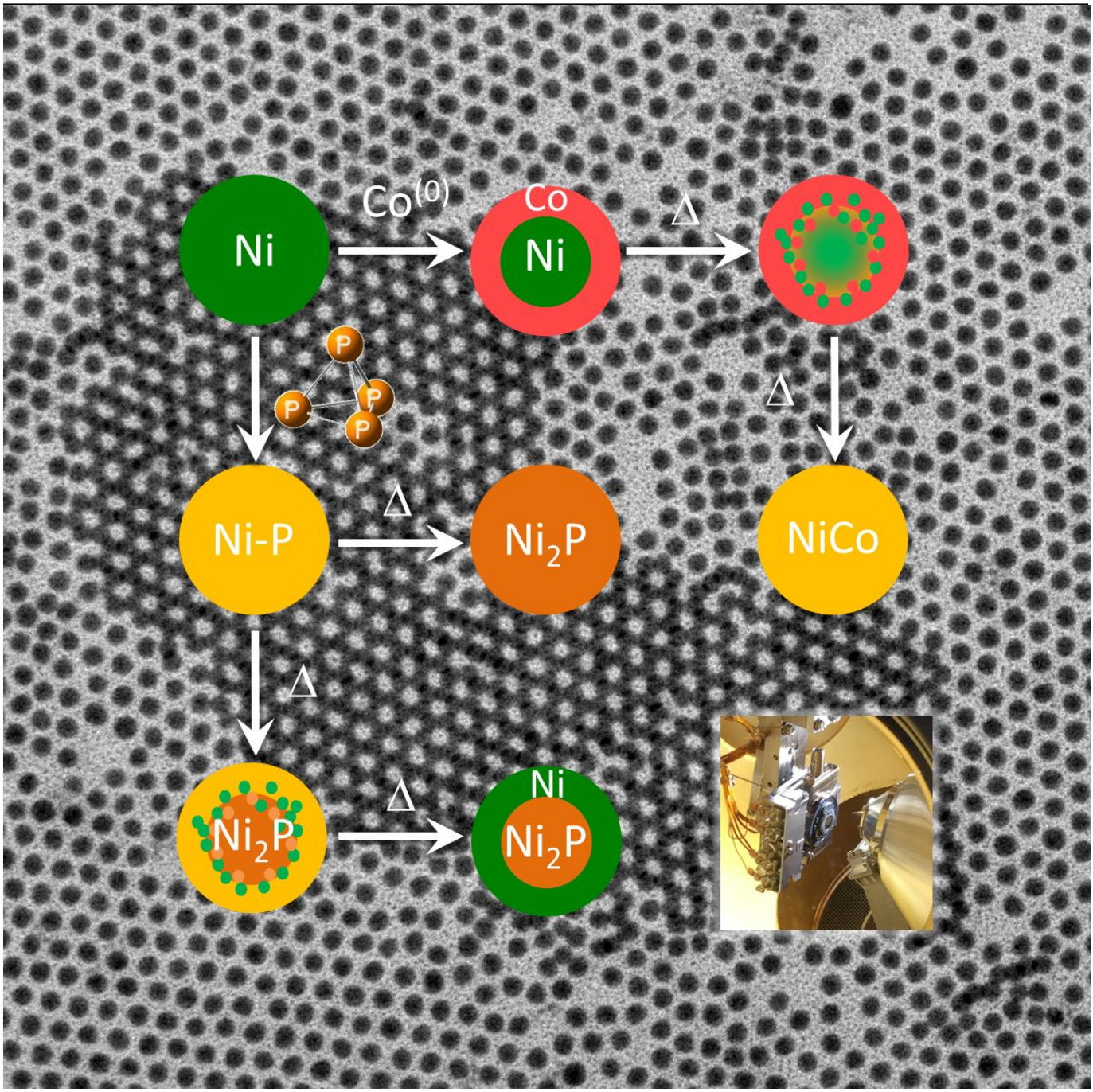

Abstract: Designing well-defined nanoparticles and nanoalloys is a tremendous way to achieve in-depth understanding of their intrinsic properties. In particular, structure and composition of the core and the surface of nanoalloys can be investigated by a combination of state-of-the-art *in situ* microscopy and spectroscopy. These nanoalloys represent a playground to establish structure-properties relationships within the nano-matter. They provide a much needed understanding of the distribution of each element within the nanoparticles, depending on the environment (gaseous atmosphere, temperature, etc.). This distribution may evolve over time. Lighter elements, such as phosphorus, are critical to the reactivity of the nanoparticle's surface in reactions such as CO or CO_2 hydrogenation. Here, the rational design of nanoalloys will be discussed (reactants choice, composition control), in relation with their surface state. Consequences on heterogeneous and homogeneous catalytic reactions, as well as for energy storage and conversion, will be illustrated through examples.

1. Introduction

Metal nanoparticles and nanoalloys represent a mature research field: since the early works on gold nanoparticles,[1] many research groups joined the quest for advanced nanoparticles. These nanoparticles combine shape and size-control with increased complexity in terms of composition and element distribution inside the object (eg. core-shell or gradient nanoparticles).[2] They found applications in several fields, beyond metallurgy: catalysis,[3,4] electrocatalysis,[5] magnetism,[6,7] optics[8] and plasmonics,[9] biology[10] and nano-medecine, etc.[2]
Nowadays, the bulk of the research still deals with optimizing nanoparticles morphology, crystal structure and composition, with an effort on including light elements in metals (eg. phosphorus,[11,12] carbon,[13,14] boron[11,15]). In this purpose, synthetic routes have been diversified: reaction triggers include microwave and sonochemistry and reaction media expanded from aqueous and organic solutions to ionic liquids and molten salts.[16]
However, these only address one side of the coin: the features of the nanoparticle core. The second side is the nature of the surface. As established for decades in metallurgy, surface of alloys may differs from the bulk, first because a passivation hydroxylated layer forms on many metals exposed to ambient conditions, second because many metal surfaces reconstruct spontaneously: the surface structure differs from the bulk, from a crystallographic standpoint. In nanoalloys, surface and core both weight in, because surface energy is comparable to lattice energy in these small objects. As a consequence, design and application of nano-scaled alloys should take great care to define and control their surface state: (i) composition of the top layers, (ii) crystallographic organization of these layers and (iii) presence of organic or inorganic stabilizing agents bound to the shell. Due to the high reactivity of surfaces, these parameters evolve with the environments that surround the nanoparticles, eg. aqueous solution, vacuum or atmospheric conditions.
Moreover, surface energy may also control the formation of a particular crystallographic phase and override the bulk energy. While this was well-described in the field of metal oxides – with the seminal example of TiO_2 that crystallizes into anatase instead of rutile below a critical size of ca 10 nm, this is still an active research topic for metals and metal alloys. Outcome will be a better understanding of the nanoparticle properties but also the possibility to target metastable phases and new phases absent in the bulk phase diagram. Smarter design of catalysts and electrocatalysts is also expected from this research.
The critical steps to explore these questions are (i) to develop model systems: nanoparticles with controlled composition and surface state, and (ii) to watch them evolve under controlled conditions using *in situ* spectroscopy. In this personal account, this two-step methodology will be discussed through selected examples taken from resent research.

2 Designing metal nanoparticles and nanoalloys

2.1 Nickel nanoparticles with controlled size and surface chemistry

The example of nickel nanoparticles synthesis illustrates how to choose rationally the reactants and reaction temperature. In a broadly-used synthesis, $Ni(acac)_2$ (acac = acetylacetonate) is reacted with oleylamine (OAm) and tri-n-octylphosphine (TOP) under air-free conditions to form nickel(0) nanoparticles (Figure 1).[17–19] This reaction is minimal in complexity as it employs only three reactants.

[a] Dr. S. Carenco,
Sorbonne Université, CNRS, Collège de France, Laboratoire de Chimie de la Matière Condensée de Paris
4 place Jussieu, 75252 Paris Cedex 05
E-mail: sophie.carenco@sorbonne-universite.fr

Sophie Carenco graduated in 2008 from *Ecole Polytechnique* in France. She obtained her PhD in 2011 from *Sorbonne Université-UPMC*, Paris. From 2012 to 2013, she was a post-doctoral fellow at *Lawrence Berkeley National Lab*, Berkeley, California. In 2014, she joined *CNRS* as a researcher in the *Laboratory of Chemistry of the Condensed Mater* at *Sorbonne Université*. She works on developing novel synthetic routes for nanoparticles (metals, metal phosphides, metal oxysulfides, metal carbides) of controlled composition and surface state, with applications in catalysis. She was awarded the *European Young Chemist Award* in 2010, the *C'Nano National Award* in 2012, the *L'Oreal-UNESCO Fellowship* in 2014 and an *ERC Starting Grant* in 2017. She is also involved in scientific outreach and published in 2012 a book about nanomaterials and chemistry.

In addition to the Ni(II) source, oleylamine serves as the reducing agent. If its stoichiometry (*x*) is higher than 4, the reaction is quantitative *vs.* nickel.[20] TOP serves as the main surface ligands: increasing its stoichiometry (*y*) results in decreasing the nanoparticles diameter.[19]

This reaction is interesting in two regards. First, it is straightforward to conduct and provides nickel nanoparticles with a yield close to 100% without complex separation procedure or size-selective centrifugation. Size control is robust (though it depends on the chemical impurities of TOP, hence on the provider company[21]). Second, its simplicity allows an in-depth understanding of the mechanism involved in the formation of Ni(0) species, the nucleation of the nanoparticles and the ripening processes. This second point is critical in the framework of designing nanoalloy synthesis.

Reaction temperature. Differential thermal analysis highlighted that nickel is reduced at 212 °C in an endothermic process.[20] The reaction temperature of 220 °C, found empirically, is in fact the optimal one that allows the quantitative reduction of Ni(II) while minimizing the inclusion of carbon (as carbide)[22] and phosphorus (as phosphide)[23,24] in the forming nanoparticles. Yet, at this temperature the reduction is swift (completed in the first minutes), resulting in a burst of nucleation and favoring a narrow size dispersion.

Byproducts. Analysis of the reaction supernatant and DFT modeling of the first steps of the reaction allow identifying the formation of several byproducts (Figure 1 bottom),[20] which can also remain on the surface of the nanoparticles as ligands.

Ripening processes. Aliquots taken from the solution at 220 °C showed that a reaction time of 2h was optimal to complete the growth of the nanoparticles. After 2h, ripening processes start affecting the morphology and size distribution of the nanoparticles, because TOP promotes the formation of Ni(0) complexes (leaching) at elevated temperature.[19]

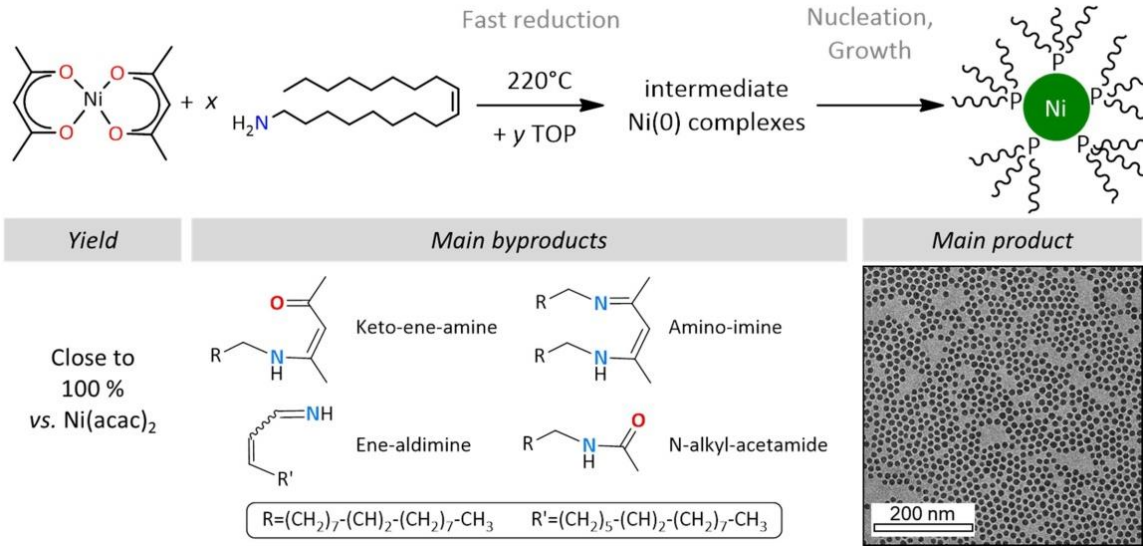

Figure 1. (Top) Synthesis of nickel nanoparticles from a nickel(II) precursor, oleylamine and tri-n-octylphosphine. (Bottom) Main organic byproducts and TEM of nickel nanoparticles.

From a design viewpoint, one should take into account the information displayed on the left side of Figure 1 (yield and byproducts), rather than focusing only on the right side (main product). This allows anticipating the possibilities and limitations of the system beyond the usual criteria of size distribution and morphology. Here, the synthesis shows interesting features: a quantitative yield, limited ripening processes over a 2-hour period and a relatively limited number of organic byproducts. A second reaction could thus be envisioned directly on the crude solution, to form bimetallic NiCo nanoparticles.

2.2 Nickel-cobalt nanoparticles: from core-shell to alloys

Core-shell nanoparticles have found technological applications in several fields, eg. luminescence and magnetism.[25] They also serve as a model system of nano-reactors to study reactions over limited length scale.

Stoichiometry and composition. To build a cobalt shell around nickel nanoparticles, a cobalt molecular precursor is introduced in a colloidal solution of nickel nanoparticles. It should preferably be at oxidation state 0 to avoid galvanic replacement of Ni by Co and the etching of the starting nickel nanoparticles, and it should be soluble in the reaction medium that mostly contains oleylamine. $Co_2(CO)_8$ was selected accordingly, as it was shown to form Co(0) nanoparticles in a hot-injection procedure.[26] It was later showed that heating-up and hot-injection procedures give equivalent results.[27] Moreover, the precursor decomposition is a clean and almost quantitative reaction. Thus, the final Ni:Co ratio can be controlled *a priori* from the reactants stoichiometry. This was verified by energy dispersive spectroscopy (EDS) mapping of the nanoparticles in scanning-transmission electron microscopy (STEM), a technique well-suited to the analysis of local composition at the nanoscale.[28] Nanoparticles with Ni:Co ratio of 1:1 and 1:4 were studied. As expected, the shell was thicker in the second case than in the first.[29]

Reaction temperature. The reaction temperature was carefully selected in this reaction: previous works had shown that cobalt nanoparticles nucleated in the solution at 180 °C.[27] Because homogeneous nucleation in the solution is disfavored over heterogeneous nucleation on an existing surface, a lower temperature was used in the first 10 minutes of the reaction, promoting the formation of the first layers of the cobalt shell

(Figure 2 – for clarity, organic ligands were omitted from this figure and the following ones). The temperature was then increase to 180 °C and maintained for one hour in order to fully react the Co(0) precursor with the nickel nanoparticles. After isolation from the reaction medium by centrifugation, the nanoparticles presented a core-shell morphology with nickel in the core and cobalt in the shell (Figure 2).[30] By design, it is possible to control independently the core diameter (cf. previous section about nickel nanoparticles) and the shell thickness, by adjusting the cobalt precursor stoichiometry.

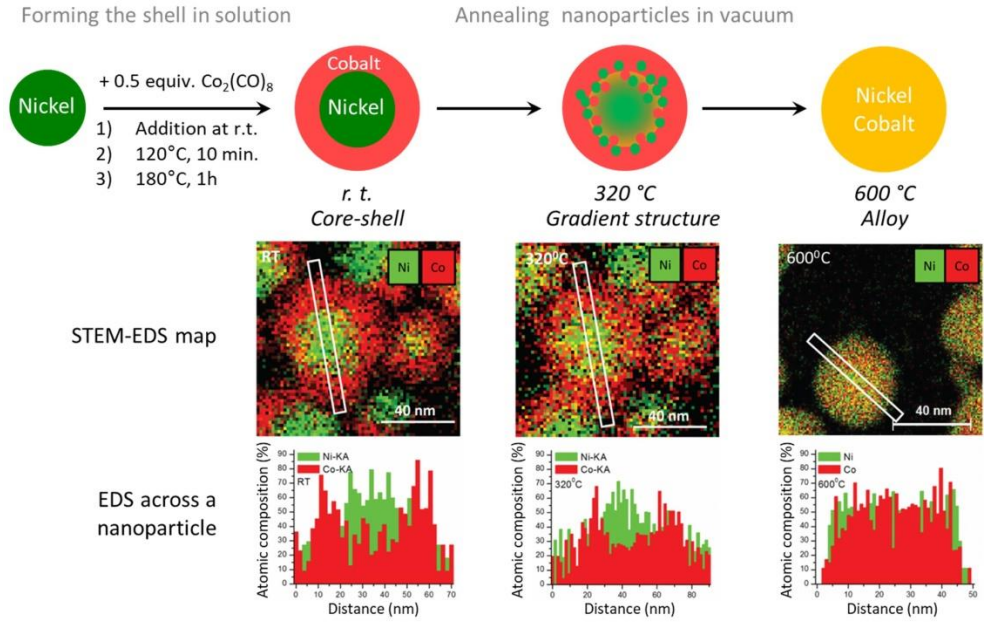

Figure 2. (Top) Synthesis of nickel-cobalt core-shell nanoparticles and their structural evolution upon annealing under vacuum. (Bottom) STEM-EDS maps and EDS measurements across nanoparticles. NB: organic ligands were omitted.

Surface reactivity of the nanoparticles was high when the shell of cobalt was present: a thin layer of *ca* 1 nm of amorphous cobalt oxide formed as soon as the nanoparticles where exposed to ambient conditions, as showed by both X-ray photoelectron spectroscopy (XPS) and EDS.[30]

Interestingly, annealing the nanoparticles under vacuum promoted a reordering within each nanoparticle, eventually yielding alloyed structures. This was demonstrated using STEM-EDS equipped with a heating stage. At 320 °C, the limit between nickel and cobalt region started to blur, indicating a gradient of composition at the core-shell interface (Figure 2 bottom). Similar distribution of Ni and Co, indicating the formation of an alloy, was observed when the temperature reached 550 °C and confirmed at 600 °C.[30]

This example of two-step one-pot synthesis Ni-Co bimetallic nanoparticles could in principle be extended to any metal, with a higher chance of success when selecting metal precursor at an appropriate oxidation state (here, 0), that decomposes in a quantitative reaction at a temperature compatible with the survival of the nanoparticles formed in the first step. Whether the second step results in a core-shell structure or an alloy structure will depend on the miscibility of the two metals and on the energy barrier for the incoming metal to diffuse in the preformed nanoparticle core. In the present case, nickel and cobalt can form an alloy at the ratio used (according to the bulk phase diagram) but diffusion of cobalt in the nickel core started at a temperature of 320 °C, much higher that the reaction temperature. The core-shell structure can thus be considered to be a metastable one, formed under kinetic control.

In the following section, incorporation of lighter elements (carbon and phosphorus) in nickel nanoparticles will be discussed, as it experimentally happens at lower temperatures, in the range 150–300 °C.

2.3 Metal and lighter elements: the cases of nickel carbides and nickel phosphide.

Carbon and phosphorus both form covalent bonds with transition metals. Phase diagrams indicate a variety of phases, such as Ni_3C and Ni_2P. Nanoscaled metal carbides and metal phosphides are being investigated in many fields, such as electrocatalysis.[31,32]

Fortuitous insertion of carbon[22] and phosphorus[23,29,33] in transition metal nanoparticles was observed, due to the partial decomposition of the organic reactants (oleylamine, 1-octadecene, TOP, etc.) during the synthesis. These decomposition pathways are not quantitative but allowed obtaining Ni_3C_{1-x} nanoparticles covering the whole range of x from 0 to 1,[22] and forming several phases of metal phosphide nanoparticles, such as Cu_3P,[34] Co_2P and CoP,[35] $Ni_{12}P_5$ and Ni_2P.[36] Carbon and phosphorus insertion are obtained in similar temperature range (150 – 300 °C) and reaction medium.[24] It is therefore difficult to assert that syntheses using TOP produce carbon-free phosphides, especially in the case of nickel, into which carbon is highly soluble. Because composition analysis of the carbon is difficult, many studies rely on x-ray diffraction (XRD) on powder to assign the phases and then the composition. Few surprising results should however be pointed out, such as the fact that $Ni_{12}P_5$ forms at 350 °C preferentially over Ni_2P upon increasing of the oleylamine stoichiometry from 3 to 22.5 equiv. vs. nickel.[36] Oleylamine is a source of carbon in these conditions:[22] tone cannot exclude that the phase obtained is

isostructural to $Ni_{12}P_5$ but contains significant amounts of carbide species. A spectroscopy sensitive to carbide species, such as X-ray absorption near edge structure (XANES) at carbon K-edge, might clarify this point.

Because of the difficulties inherent to working with TOP, a phosphorus source that is also a source of carbon,[24] other precursors were explored,[37] such as white phosphorus P_4. This molecule is highly reactive, at the proper oxidation state (0) to react with a metal(0) precursor, and soluble in the reaction medium. The proof of concept was established by comparing the reactivity of a Ni(0) complex with these of preformed Ni(0) nanoparticles: in both case, P_4 was found to be a stoichiometric phosphorus donor, forming Ni_2P when 1/8 equiv. was introduced.[38] This route was generalized to other metals such as In, Cu, Fe and Pd.[39–42,43]

The P_4 route presents the advantage of retaining the same set of organic ligands around the nanoparticles: in the case of nickel, mostly TOP and oleylamine-derived molecules (see Figure 1). Ni_2P nanoparticles were investigated as active material in negative electrode of Li-ion batteries, in order to provide insights on the so-called conversion mechanism that was observed for other metal phosphides.[44] With the native organic shell, nanoparticles were electronically insulating, thus inactive. Knowing the composition of this shell, calcination under inert atmosphere was expected to produce a carbon-rich conductive layer. This was experimentally verified through the observation of a low-contrast shell by TEM and of a carbon layer by XPS.[45] Moreover, thanks to the low size dispersion of the initial nanoparticles, newly-formed nickel nanoparticles of smaller diameter could be identified as the results of the conversion reaction occurring during the discharge of the battery: $Ni_2P + 3\ Li \rightarrow 2Ni + Li_3P$.

2.4 From elucidation of reaction mechanism to the design of core-shell structure for magnetic and catalytic applications.

Step-by-step analysis of the reaction of P_4 on fcc nickel nanoparticles showed the formation of an amorphous intermediate at a temperature as low as 120 °C (Figure 3).[46] Upon further heating, the evolution of this amorphous compound depends on the stoichiometry of phosphorus *vs.* Ni. One would expect that this route provides access to all phases described in the bulk phase diagram:[47] Ni_3P, $Ni_{12}P_5$, Ni_5P_2, NiP_2, etc. Selecting different phases was successful for other metals (eg. Pd, Cu), yet with less variety than expected from the bulk phase diagrams.[40,48] In the case of nickel, this route only allowed the crystallization of Ni_2P hexagonal phase (Figure 3). When P_4 was introduced with a lower stoichiometry, phosphorus-poor phases (Ni_3P, $Ni_{12}P_5$) did not crystallize. Rather, a Ni_2P core started to crystallize at 150 °C. Eventually, all phosphorus atoms migrated to this core and the remaining of the nanoparticles (nickel) crystallized at 220 °C (Figure 3 bottom). Besides, NiP_2 could be obtained at higher temperature but the nanoparticles size was not preserved.

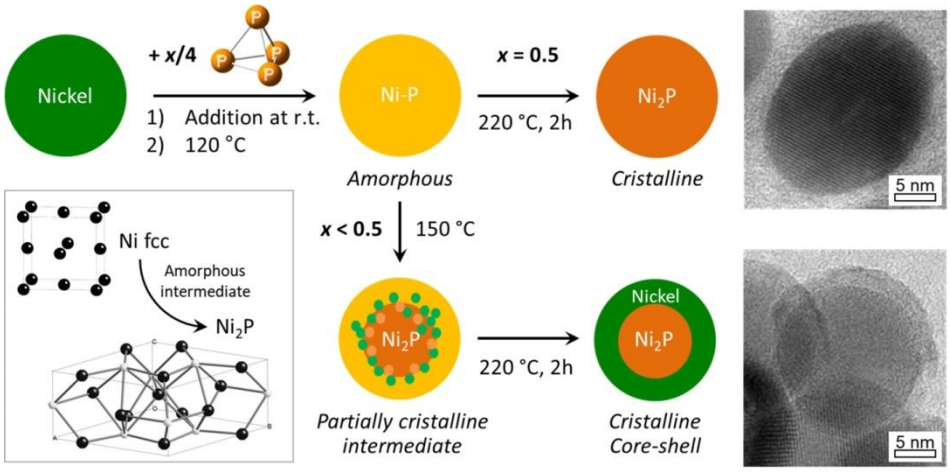

Figure 3. (Top) Synthesis of Ni_2P nanoparticles from Ni(0) nanoparticles. (Bottom) Synthesis of core-shell Ni_2P-Ni nanoparticles. (Inset) Crystal structures of Ni fcc and Ni_2P.

This unexpected result opened a new route for designing core-shell structures: here, the stoichiometry of phosphorus ultimately controls the relative volume of the core and the shell in the nanoparticles. Reaction with less phosphorus led to a thicker nickel shell. Because metallic nickel is ferromagnetic and Ni_2P is not, the nanoparticles with thicker shells presented a higher magnetization at saturation than those with a larger core, all other parameters (nanoparticles diameter, etc.) being equal.[46]

Moreover, the catalytic properties of the nanoparticles were also related to their phosphorus content. Alkynes hydrogenation was performed in solution at 80 °C: the selectivity for alkenes vs. alkanes was high with Ni_2P catalysts, low with Ni(0) nanoparticles and intermediate for the core-shell structure with an average composition of Ni_3P.[49] In this latter case, selectivity actually increased over time. This suggests that some phosphorus from the inner layer may have migrated back to the surface, making it alike Ni_2P.

Beyond these two applications, core-shell Ni_2P-Ni structure are an exciting case of study: phase speciation was influenced by the nanoscale, highlighting a need for phase diagrams that take into account the surface energy of nanoalloys.[48] Beyond these thermodynamic considerations, the difficulty – and opportunity – when dealing with nanoalloys is the huge amount of available surface that is affected by the environment. In the next section, the monitoring of nanoalloys exposed to reactive gases is discussed.

3. *In situ* monitoring of nanoparticles and nanoalloys under environmental conditions

Most analytical techniques that involve electron guns or analyzers operated under high voltages cannot be operated under a gas pressure in a straightforward manner. Conditions of analysis of the materials differ from conditions of utilization: this is called the pressure gap. Fortunately, instruments have evolved in line with the demands of materials scientists and now propose technical answers to bridge the pressure gap. These analyses are often referred to as "environmental".

3.1 Selected tools in the arsenal of environmental analysis

Transmission electron microscopy (TEM). For the analysis of nanoscale objects, electron microscopy naturally comes to mind. Modern instruments combine structural and chemical capabilities, thanks to high-resolution imaging, energy dispersive analysis (EDS) and electron energy loss spectroscopy (EELS) that operate in regular or scanning modes.[28] Figure 2 illustrates the monitoring of NiCo nanoparticles during annealing: these measurements were performed *in situ*, but under ultra-high vacuum (UHV).

Technological breakthroughs have allowed the introduction of gas directly in the TEM column (environmental TEM) up to *ca* 20 mbar. Moreover, sample-holders can nowadays integrate gas or liquid cells that withstand a pressure of 1 bar.[50,51] They rely on thin windows of fairly transparent materials (eg. Si_3N_4) to separate the high-pressure region from the UHV of the column. Interestingly, X-ray spectroscopies have also explored these two paths: increasing the pressure in the whole analysis chamber or confining the high-pressure region to a limited volume.

X-ray photoelectron spectroscopy (XPS). XPS informs on the surface state of nanoparticles and nanoalloys. By collecting the electrons close to the sample and limiting their interaction with gas molecules through differential pumping stages, the pressure in the analysis chamber was increased from UHV to *ca* 20 mbar (Figure 4 left).[52] The pressure is still low compared to these used in heterogeneous catalysis but it allows saturation of the sample surface with gas molecules. Near-ambient-pressure XPS (NAP-XPS) instruments are available at several synchrotrons but can also be operated with a laboratory x-ray source. Alternative developments rely on small reaction chambers (called cells) which are directly mounted on the hollow cone that serves to collect electrons.[52]

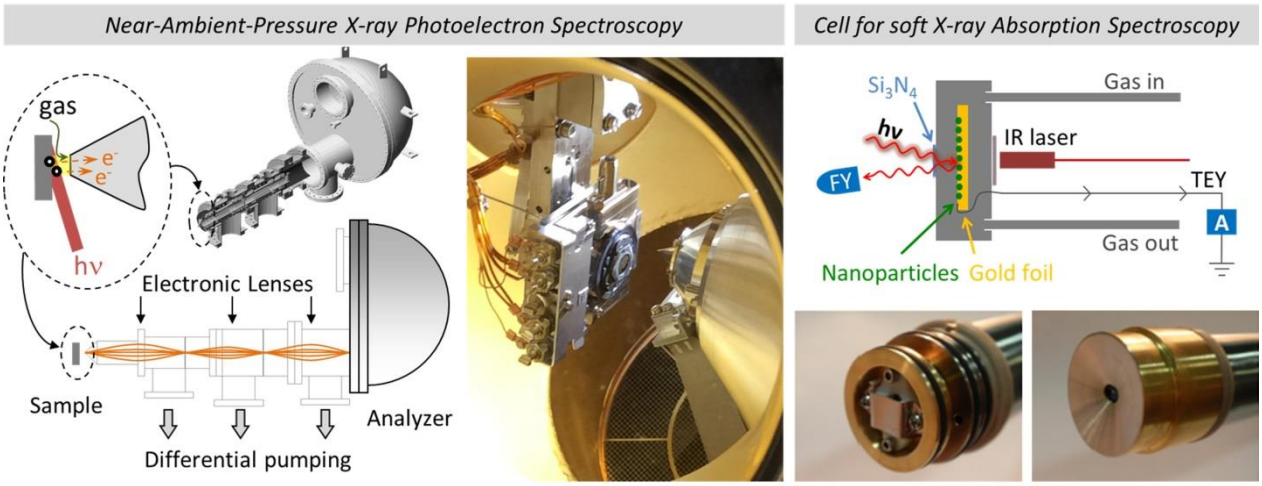

Figure 4. (Left) Operating principle of NAP-XPS and a view of the analysis chamber at Soleil synchrotron. (Right) Operating principle for X-ray absorption spectroscopy with soft x-rays and two views of a cell head (without and with its protective cap) developed at the Advanced Light Source synchrotron.[53]

X-ray absorption spectroscopy (XAS). This spectroscopy is most often operated with hard x-rays (above 5 keV). In this case, operating under environmental conditions is convenient because of the low attenuation of the incoming and outgoing X-rays in a 1 bar atmosphere and through thick windows of beryllium or glass, regardless of the detection mode (transmission or fluorescence). However, XAS with soft x-rays (less than *ca* 1.5 keV) and tender x-rays (*ca* 1.5 to 5 keV) is also interesting as it give access to L-edges of first-raw transition metals and to K edges of lighter elements such as carbon, oxygen, and phosphorus.[54] Because of the higher attenuation of the incoming beam, operating under vacuum is required. Like for TEM, gas cells[53] and liquid cells[55] were thus developed, using thin membranes such as Si_3N_4 to separate the sample from the vacuum (Figure 4 right). The nanoparticles are deposited on a substrate and exposed to a chosen gas mixture at a pressure of 1 bar or less. Back-side laser heating allows controlling the temperature. Interestingly, these types of cells allow measurements in two modes. Total fluorescence yield (FY) is obtained from a detector near the cell window and provides information on the whole nanoparticles volume. Total electron yield (TEY) is collected through the substrate and amplified. It is typically sensitive to the first layers of a solid, i.e. the surface of the nanoparticles. TEY was particularly useful for identifying the formation of surface cobalt oxide from cobalt nanoparticles exposed to CO and H_2 (as a model of the Fischer-Tropsch synthesis).[56]

While each environmental techniques described above provides invaluable insights on the surface and core of nanoparticles, combining local (TEM) and ensemble (XAS and XPS) measurements is best suited to fully understand the transformations of nanoalloys.[57]

3.2 Reactivity of bimetallic nanoparticles exposed to gas

Metal surfaces exposed to gas such as CO are prone to reconstruct.[58,59] When they contain several elements, overall surface energy as well as the affinity of the elements for the incoming molecules may trigger deep transformations such as atoms migration from buried layers. This was identified in several nanoalloys, such as RhPd and PdPt.[60]

In this context, nanoparticles of well-defined composition and structure, as described above, are excellent model systems. Cycles of oxidation (under O_2) and reduction (under H_2) inform on the potential transformation of the nanoparticles in the context of catalysis. On Ni-Co core-shell nanoparticles, formation of NiCo surface alloy was observed at temperatures as low as 220 °C using pressures of 1.33 mbar for O_2 and 6.66 mbar for H_2.[29] This temperature is significantly lower than these of the alloying process under vacuum. The process was followed by XPS that indicated an increasing Ni:Co surface ratio upon cycling (Figure 5 right). Interestingly, this alloying process was accompanied with the partial hollowing of the original nickel core, due to volume differences between the oxidized and reduced state, and to the diffusion of nickel from the core to the shell.

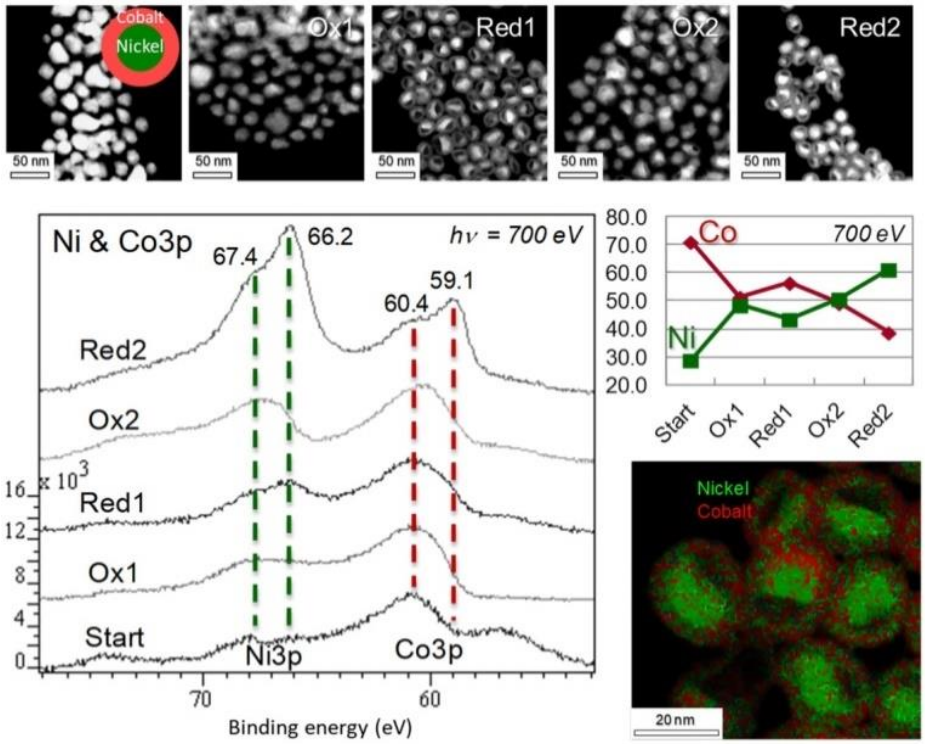

Figure 5. Ni-Co core-shell nanoparticles exposed to two cycles of oxidation (ox) and reduction (red). (Top) *Ex situ* STEM in high-angle annular dark field mode. (Left) NAP-XPS of Ni 3p and Co 3p regions. (Top right) Relative amount of Co and Ni at the surface (in %). (Bottom right) STEM-EDS of the nanoparticles after the two cycles.

Bimetallic CuCo nanoparticles were also studied with the same strategy (Figure 6).[61] In this case, high-pressure analysis at 1 bar was conducted in the cell described in Figure 4 (right), in combination with XPS. XAS allowed following the successive formation of CoO then Co_3O_4 upon oxidation (Figure 6 left). Full reduction of the cobalt was possible under 1 bar at 250 °C. NAP-XPS showed that both cobalt and copper underwent oxidation then reduction upon cycling. Under reducing conditions, the surface was slightly more cobalt-rich than under oxidizing conditions (Figure 6, top right).

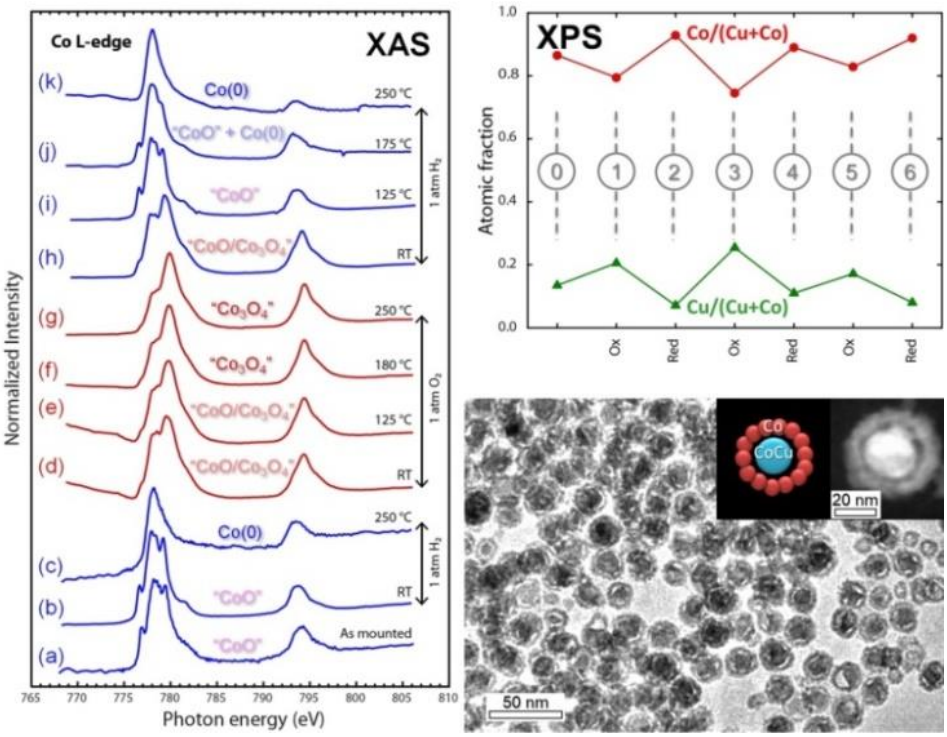

Figure 6. CuCo bimetallic nanoparticles exposed to three cycles of oxidation (ox) and reduction (red). (Left) XAS at Co L-edge under 1 bar of gas. (Top right) Surface atomic fractions of Cu and Co obtained from XPS of Cu 2p and Co 2p regions. (Bottom right) TEM of the initial CuCo nanoparticles.

The two examples described above illustrate the variety of behaviors that are encountered in bimetallic nanoparticles. State-of-the-art spectroscopy and microscopy were the cornerstone of these studies as they allowed to analyze both the core and the surface of the nanoparticles, step by step. Reaction mechanisms could be proposed thanks to the use of well-defined starting nanoparticles, as model systems.

Further efforts should be pursued in order to monitor the adsorbates that are bound to the nanoparticles surface during a catalytic reaction. On the CuCo nanoparticles exposed to syngas (CO and H_2), CO adsorption, CO dissociation and formation of surface hydroxyls was observed.[61] Unfortunately, the nanoparticles segregated upon this treatment and the initial structure was lost. On the opposite, the NiCo nanoparticles did not further evolve when exposed to CO_2 and H_2. Under catalytic conditions, formaldehyde (at 200 °C) and methanol (at 350 °C) were formed along the main product, CO. This was a direct consequence of the surface composition of the nanoparticles.[29]

In addition to monitoring the adsorbates, it seems critical to follow the evolution of surface ligands, when these are not burnt by the oxidation-reduction cycles performed before the catalytic reaction. Instead, organic ligands could modulate the properties of the nanoparticle's surface. XPS showed that bare ruthenium nanoparticles prepared by reduction of RuO_2[62] presented more reduced Ru surface atoms than diphosphine-covered ruthenium nanoparticles.[63] The P 2p region analyzed by NAP-XPS allowed monitoring the partial degradation of the phosphine during the CO methanation reaction. These results show the feasibility of monitoring organic ligands at the surface of nanoparticles.

In addition to the experimental approaches described above, computational methods may also provide structural prediction of segregation within nanoparticles. This was exemplified on the case of PtNi nanoparticles, active in oxygen reduction reaction.[64,65,66]

4. Summary and Outlook

The design of metal nanoparticles and nanoalloys was discussed. Choices of reaction precursors, temperature and surface ligands were detailed in few examples of quantitative reactions, such as the formation of nickel, nickel-cobalt and nickel phosphide nanoparticles. A special care was taken to illustrate how and why the surface state should be adequately described when dealing with nanoscale objects. In this purpose, operating principles of environmental characterization tools such as TEM, XPS and XAS were discussed and illustrated with cobalt, ruthenium, nickel-cobalt, and copper-cobalt nanoparticles. Consequences of the core and surface compositions on the magnetic and catalytic properties were shown. In all the cases discussed here, the combination of low size-dispersity, well-defined surface state and tunable composition was critical to the straightforward use of the nanoparticles in relation with their specific properties (magnetic, catalytic, etc.).

Future of the field probably lays in increasing the complexity of these objects, eg. by pursuing ternary compounds and the insertion of lighter elements in alloys, such as carbon[14] or boron,[57,67] through innovative routes. In the development of catalysts and devices, coupling of environmental techniques described here with others, more sensitive to organic surface species, such as infra-red spectroscopies (eg. diffuse reflectance infrared Fourier transform spectroscopy and polarization modulation infrared reflection adsorption spectroscopy), should also help make surface ligands an asset

rather than a barrier. Finally, further development of modeling approaches that include ligands and organic surface molecules on top of the inorganic core would be a great help.

Acknowledgements

Sorbonne Université, CNRS and Collège de France are acknowledged for financial support. S.C. gratefully acknowledges co-authors of the works described in this Personal Account.

Keywords: nanoparticles • nanoalloys • core-shell • x-ray spectroscopy • metal phosphides • surface reactivity

(1) Haruta, M.; Kobayashi, T.; Sano, H.; Yamada, N. Novel Gold Catalysts for the Oxidation of Carbon Monoxide at a Temperature Far below 0.DEG.C. *Chem. Lett.* **1987**, No. 2, 405–408.

(2) Ghosh Chaudhuri, R.; Paria, S. Core/Shell Nanoparticles: Classes, Properties, Synthesis Mechanisms, Characterization, and Applications. *Chem. Rev.* **2012**, *112* (4), 2373–2433.

(3) Wang, D.; Li, Y. Bimetallic Nanocrystals: Liquid-Phase Synthesis and Catalytic Applications. *Adv. Mater.* **2011**, *23* (9), 1044–1060.

(4) Jia, C.-J.; Schüth, F. Colloidal Metal Nanoparticles as a Component of Designed Catalyst. *Phys. Chem. Chem. Phys.* **2011**, 2457–2487.

(5) You, H.; Yang, S.; Ding, B.; Yang, H. Synthesis of Colloidal Metal and Metal Alloy Nanoparticles for Electrochemical Energy Applications. *Chem. Soc. Rev.* **2013**, *42* (7), 2880–2904.

(6) Reddy, L. H.; Arias, J. L.; Nicolas, J.; Couvreur, P. Magnetic Nanoparticles: Design and Characterization, Toxicity and Biocompatibility, Pharmaceutical and Biomedical Applications. *Chemical Reviews*. 2012, pp 5818–5878.

(7) Lu, A.-H.; Salabas, E. L.; Schüth, F. Magnetic Nanoparticles: Synthesis, Protection, Functionalization, and Application. *Angew. Chem. Int. Ed. Engl.* **2007**, *46* (8), 1222–1244.

(8) Smith, A. M.; Mohs, A. M.; Nie, S. Tuning the Optical and Electronic Properties of Colloidal Nanocrystals by Lattice Strain. *Nat. Nanotechnol.* **2009**, *4* (1), 56–63.

(9) Christopher, P.; Xin, H.; Linic, S. Visible-Light-Enhanced Catalytic Oxidation Reactions on Plasmonic Silver Nanostructures. *Nat. Chem.* **2011**, *3* (6), 467–472.

(10) De, M.; Ghosh, P. S.; Rotello, V. M. Applications of Nanoparticles in Biology. *Adv. Mater.* **2008**, *20* (22), 4225–4241.

(11) Carenco, S.; Portehault, D.; Boissière, C.; Mézailles, N.; Sanchez, C. Nanoscaled Metal Borides and Phosphides: Recent Developments and Perspectives. *Chem. Rev.* **2013**, *113* (10), 7981–8065.

(12) Ye, E.; Zhang, S.-Y.; Lim, S. H.; Bosman, M.; Zhang, Z.; Win, K. Y.; Han, M.-Y. Ternary Cobalt-Iron Phosphide Nanocrystals with Controlled Compositions, Properties, and Morphologies from Nanorods and Nanorice to Split Nanostructures. *Chemistry* **2011**, *17* (21), 5982–5988.

(13) Pol, V. G.; Pol, S. V; Gedanken, A. Dry Autoclaving for the Nanofabrication of Sulfides, Selenides, Borides, Phosphides, Nitrides, Carbides, and Oxides. *Adv. Mater.* **2011**, *23* (10), 1179–1190.

(14) Ressnig, D.; Moldovan, S.; Ersen, O.; Beaunier, P.; Portehault, D.; Sanchez, C.; Carenco, S. An Expeditious Synthesis of Early Transition Metal Carbide Nanoparticles on Graphitic Carbons. *Chem. Commun.* **2016**, *52* (61), 9546–9549.

(15) Portehault, D.; Devi, S.; Beaunier, P.; Gervais, C.; Giordano, C.; Sanchez, C.; Antonietti, M. A General Solution Route toward Metal Boride Nanocrystals. *Angew. Chem. Int. Ed. Engl.* **2011**, *50* (14), 3262–3265.

(16) Rao, C. N. R.; Ramakrishna Matte, H. S. S.; Voggu, R.; Govindaraj, A. Recent Progress in the Synthesis of Inorganic Nanoparticles. *Dalt. Trans.* **2012**, *41* (17), 5089.

(17) Park, J.-G.; Kang, E.; Son, S. U.; Park, H. M.; Lee, M. K.; Kim, J.; Kim, K. W.; Noh, H.-J.; Park, J.-H.; Bae, C. J.; Hyeon, T. Monodisperse Nanoparticles of Ni and NiO: Synthesis, Characterization, Self-Assembled Superlattices, and Catalytic Applications in the Suzuki Coupling Reaction. *Adv. Mater.* **2005**, *17* (4), 429–434.

(18) Winnischofer, H.; Rocha, T. C. R.; Nunes, W. C.; Socolovsky, L. M.; Knobel, M.; Zanchet, D. Chemical Synthesis and Structural Characterization of Highly Disordered N Colloidal Nanoparticles. *ACS Nano* **2008**, *2* (6), 1313–1319.

(19) Carenco, S.; Boissière, C.; Nicole, L.; Sanchez, C.; Le Floch, P.; Mézailles, N. Controlled Design of Size-Tunable Monodisperse Nickel Nanoparticles. *Chem. Mater.* **2010**, *22* (4), 1340–1349.

(20) Carenco, S.; Labouille, S.; Bouchonnet, S.; Boissière, C.; Le Goff, X.-F.; Sanchez, C.; Mézailles, N. Revisiting the Molecular Roots of a Ubiquitously Successful Synthesis: Nickel(0) Nanoparticles by Reduction of [Ni(acetylacetonate)(2)]. *Chem. Eur. J.* **2012**, *18* (44), 14165–14173.

(21) Carenco, S. PhD Thesis. A New Versatile Route to Metal Phosphide Nanoparticules Using White Phosphorus : Applications in Catalysis and for Lithium Batteries, UPMC, 2011.

(22) Schaefer, Z. L.; Weeber, K. M.; Misra, R.; Schiffer, P.; Schaak, R. E. Bridging Hcp-Ni and Ni 3 C via a Ni 3 C 1- X Solid Solution: Tunable Composition and Magnetism in Colloidal Nickel Carbide Nanoparticles. *Chem. Mater.* **2011**, *23* (9), 2475–2480.

(23) Moreau, L. M.; Ha, D.-H.; Bealing, C. R.; Zhang, H.; Hennig, R. G.; Robinson, R. D. Unintended Phosphorus Doping of Nickel Nanoparticles during Synthesis with TOP: A Discovery through Structural Analysis. *Nano Lett.* **2012**, *12* (9), 4530–4539.

(24) Carenco, S.; Liu, Z.; Salmeron, M. The Birth of Nickel Phosphide Catalysts: Monitoring Phosphorus Insertion into Nickel. *ChemCatChem* **2017**, *9* (12), 2318–2323.

(25) Kim, M. R.; Xu, Z.; Chen, G.; Ma, D. Semiconductor and Metallic Core-Shell Nanostructures: Synthesis and Applications in Solar Cells and Catalysis. *Chem. - A Eur. J.* **2014**, *20* (36), 11256–11275.

(26) Puntes, V. F.; Krishnan, K. M.; Alivisatos, A. P. Colloidal Nanocrystal Shape and Size Control : The Case of Cobalt. *Science (80-.).* **2001**, *291*, 2115–2117.

(27) Timonen, J. V. I.; Seppälä, E. T.; Ikkala, O.; Ras, R. H. a. From Hot-Injection Synthesis to Heating-up Synthesis of Cobalt Nanoparticles: Observation of Kinetically Controllable Nucleation. *Angew. Chem. Int. Ed. Engl.* **2011**, *50* (9), 2080–2084.

(28) Carenco, S.; Moldovan, S.; Roiban, L.; Florea, I.; Portehault, D.; Vallé, K.; Belleville, P.; Boissière, C.; Rozes, L.; Mézailles, N.; Drillon, M.; Sanchez, C.; Ersen, O. The Core Contribution of Transmission Electron Microscopy to Functional Nanomaterials Engineering. *Nanoscale* **2016**, *8* (3), 1260–1279.

(29) Carenco, S.; Wu, C.-H.; Shavorskiy, A.; Alayoglu, S.; Somorjai, G. A.; Bluhm, H.; Salmeron, M. Synthesis and Structural Evolution of Nickel-Cobalt Nanoparticles Under H 2 and CO 2. *Small* **2015**, *11* (25), 3045–3053.

(30) Bonifacio, C. S.; Carenco, S.; Wu, C. H.; House, S. D.; Bluhm, H.;

Yang, J. C. Thermal Stability of Core–Shell Nanoparticles: A Combined in Situ Study by XPS and TEM. *Chem. Mater.* **2015**, *27* (20), 6960–6968.

(31) Giordano, C.; Antonietti, M. Synthesis of Crystalline Metal Nitride and Metal Carbide Nanostructures by Sol–gel Chemistry. *Nano Today* **2011**, *6* (4), 366–380.

(32) Popczun, E. J.; McKone, J. R.; Read, C. G.; Biacchi, A. J.; Wiltrout, A. M.; Lewis, N. S.; Schaak, R. E. Nanostructured Nickel Phosphide as an Electrocatalyst for the Hydrogen Evolution Reaction. *J. Am. Chem. Soc.* **2013**, *135* (25), 9267–9270.

(33) Iablokov, V.; Beaumont, S. K.; Alayoglu, S.; Pushkarev, V. V; Specht, C.; Gao, J.; Alivisatos, A. P.; Kruse, N.; Somorjai, G. A. Size-Controlled Model Co Nanoparticle Catalysts for CO_2 Hydrogenation: Synthesis, Characterization, and Catalytic Reactions. *Nano Lett.* **2012**, *12* (6), 3091–3096.

(34) De Trizio, L.; Figuerola, A.; Manna, L.; Genovese, A.; George, C.; Brescia, R.; Saghi, Z.; Simonutti, R.; Van Huis, M.; Falqui, A. Size-Tunable, Hexagonal Plate-like Cu3P and Janus-like Cu-Cu3P Nanocrystals. *ACS Nano* **2012**, *6* (1), 32–41.

(35) Ha, D.-H.; Moreau, L. M.; Bealing, C. R.; Zhang, H.; Hennig, R. G.; Robinson, R. D. The Structural Evolution and Diffusion during the Chemical Transformation from Cobalt to Cobalt Phosphide Nanoparticles. *J. Mater. Chem.* **2011**, *21* (31), 11498.

(36) Muthuswamy, E.; Savithra, G. H. L.; Brock, S. L. Synthetic Levers Enabling Independent Control of Phase, Size, and Morphology in Nickel Phosphide Nanoparticles. *ACS Nano* **2011**, *5* (3), 2402–2411.

(37) Carenco, S.; Portehault, D.; Boissière, C.; Mézailles, N.; Sanchez, C. Nanoscaled Metal Borides and Phosphides: Recent Developments and Perspectives. *Chem. Rev.* **2013**, *113* (10), 7981–8065.

(38) Carenco, S.; Resa, I.; Le Goff, X.; Le Floch, P.; Mézailles, N. White Phosphorus as Single Source of “P” in the Synthesis of Nickel Phosphide. *Chem. Commun. (Camb).* **2008**, No. 22, 2568–2570.

(39) Carenco, S.; Demange, M.; Shi, J.; Boissière, C.; Sanchez, C.; Le Floch, P.; Mézailles, N. White Phosphorus and Metal Nanoparticles: A Versatile Route to Metal Phosphide Nanoparticles. *Chem. Commun. (Camb).* **2010**, *46* (30), 5578–5580.

(40) Carenco, S.; Hu, Y.; Florea, I.; Ersen, O.; Boissière, C.; Mézailles, N.; Sanchez, C. Metal-Dependent Interplay between Crystallization and Phosphorus Diffusion during the Synthesis of Metal Phosphide Nanoparticles. *Chem. Mater.* **2012**, *24* (21), 4134–4145.

(41) Carenco, S.; Hu, Y.; Florea, I.; Ersen, O.; Boissière, C.; Sanchez, C.; Mézailles, N. Structural Transitions at the Nanoscale: The Example of Palladium Phosphides Synthesized from White Phosphorus. *Dalt. Trans.* **2013**, *42* (35), 12667–12674.

(42) Carenco, S.; Florea, I.; Ersen, O.; Boissière, C.; Mézailles, N.; Sanchez, C. Towards Nanoscaled Gold Phosphides: Surface Passivation and Growth of Composite Nanostructures. *New J. Chem.* **2013**, 28–31.

(43) Carenco, S.; Boissière, C.; Mézailles, N.; Sanchez, C. Les Phosphures de Métaux Une Renaissance À L ’ Échelle Nanométrique. *Actual. Chim.* **2012**, *Avril*, 22–28.

(44) Boyanov, S.; Bernardi, J.; Bekaert, E.; Ménétrier, M.; Doublet, M.-L.; Monconduit, L. P-Redox Mechanism at the Origin of the High Lithium Storage in NiP 2 -Based Batteries. *Chem. Mater.* **2009**, *21* (2), 298–308.

(45) Carenco, S.; Surcin, C.; Morcrette, M.; Larcher, D.; Mézailles, N.; Boissière, C.; Sanchez, C. Improving the Li-Electrochemical Properties of Monodisperse Ni 2 P Nanoparticles by Self-Generated Carbon Coating. *Chem. Mater.* **2012**, *24* (4), 688–697.

(46) Carenco, S.; Le Goff, X. F.; Shi, J.; Roiban, L.; Ersen, O.; Boissière, C.; Sanchez, C.; Mézailles, N. Magnetic Core−Shell Nanoparticles from Nanoscale-Induced Phase Segregation. *Chem. Mater.* **2011**, *23* (8), 2270–2277.

(47) Okamoto, H. Ni-P (Nickel-Phosphorus). *J. Phase Equilibria Diffus.* **2010**, *31* (2), 200–201.

(48) Carenco, S.; Portehault, D.; Boissière, C.; Mézailles, N.; Sanchez, C. 25th Anniversary Article: Exploring Nanoscaled Matter from Speciation to Phase Diagrams: Metal Phosphide Nanoparticles as a Case of Study. *Adv. Mater.* **2014**, *26* (3), 371–390.

(49) Carenco, S.; Leyva-Pérez, A.; Concepción, P.; Boissière, C.; Mézailles, N.; Sanchez, C.; Corma, A. Nickel Phosphide Nanocatalysts for the Chemoselective Hydrogenation of Alkynes. *Nano Today* **2012**, *7* (1), 21–28.

(50) DEMBELE, K.; MOLDOVAN, S.; HIRLIMANN, C.; HARMEL, J.; SOULANTICA, K.; SERP, P.; CHAUDRET, B.; GAY, A.-S.; MAURY, S.; BERLIET, A.; FECANT, A.; ERSEN, O. Reactivity and Structural Evolution of Urchin-like Co Nanostructures under Controlled Environments. *J. Microsc.* **2018**, *269* (2), 168–176.

(51) Melinte, G.; Moldovan, S.; Hirlimann, C.; Baaziz, W.; Bégin-Colin, S.; Pham-Huu, C.; Ersen, O. Catalytic Nanopatterning of Few-Layer Graphene. *ACS Catal.* **2017**, *7* (9), 5941–5949.

(52) Starr, D. E.; Liu, Z.; Hävecker, M.; Knop-Gericke, A.; Bluhm, H. Investigation of Solid/vapor Interfaces Using Ambient Pressure X-Ray Photoelectron Spectroscopy. *Chem. Soc. Rev.* **2013**, *42*, 5833–5857.

(53) Escudero, C.; Jiang, P.; Pach, E.; Borondics, F.; West, M. W.; Tuxen, A.; Chintapalli, M.; Carenco, S.; Guo, J.; Salmeron, M. A Reaction Cell with Sample Laser Heating for in Situ Soft X-Ray Absorption Spectroscopy Studies under Environmental Conditions. *J. Synchrotron Radiat.* **2013**, *20* (3), 504–508.

(54) Zhang, H.; Wang, W.-C.; Glans, P.-A.; Liu, Y.-S.; Kapilashrami, M.; Chen, J.-L.; Chang, C.; Salmeron, M.; Escudero, C.; Pach, E.; Tuxen, A.; Chintapalli, M.; Carenco, S.; Sun, X.; Guo, J. Developing Soft X-Ray Spectroscopy for in Situ Characterization of Nanocatalysts in Catalytic Reactions. *J. Electron Spectros. Relat. Phenomena* **2014**, *197*, 118–123.

(55) Larquet, C.; Nguyen, A.-M.; Ávila-Gutiérrez, M.; Tinat, L.; Lassalle-Kaiser, B.; Gallet, J.-J.; Bournel, F.; Gauzzi, A.; Sanchez, C.; Carenco, S. Synthesis of Ce 2 O 2 S and Gd 2(1– Y) Ce 2 Y O 2 S Nanoparticles and Reactivity from in Situ X-Ray Absorption Spectroscopy and X-Ray Photoelectron Spectroscopy. *Inorg. Chem.* **2017**, *56* (22), 14227–14236.

(56) Tuxen, A.; Carenco, S.; Chintapalli, M.; Chuang, C.-H.; Escudero, C.; Pach, E.; Jiang, P.; Borondics, F.; Beberwyck, B.; Alivisatos, A. P.; Thornton, G.; Pong, W.-F.; Guo, J.; Perez, R.; Besenbacher, F.; Salmeron, M. Size-Dependent Dissociation of Carbon Monoxide on Cobalt Nanoparticles. *J. Am. Chem. Soc.* **2013**, *135* (6), 2273–2278.

(57) Gouget, G.; Debecker, D. P.; Kim, A.; Olivieri, G.; Gallet, J. J.; Bournel, F.; Thomas, C.; Ersen, O.; Moldovan, S.; Sanchez, C.; Carenco, S.; Portehault, D. In Situ Solid-Gas Reactivity of Nanoscaled Metal Borides from Molten Salt Synthesis. *Inorg. Chem.* **2017**, *56* (15), 9225–9234.

(58) Carenco, S. Carbon Monoxide-Induced Dynamic Metal-Surface Nanostructuring. *Chem. Eur. J.* **2014**, *20*, 10616–10625.

(59) Carenco, S. Observer La Surface D’ Une Nanoparticule Pendant L’ Acte Catalytique. *Actual. Chim.* **2016**, No. 557, 408–410.

(60) Tao, F.; Grass, M. E.; Zhang, Y.; Butcher, D. R.; Renzas, J. R.; Liu, Z.; Chung, J. Y.; Mun, B. S.; Salmeron, M.; Somorjai, G. a.

Reaction-Driven Restructuring of Rh-Pd and Pt-Pd Core-Shell Nanoparticles. *Science* **2008**, *322* (5903), 932–934.

(61) Carenco, S.; Tuxen, A.; Chintapalli, M.; Pach, E.; Escudero, C.; Ewers, T. D.; Jiang, P.; Borondics, F.; Thornton, G.; Alivisatos, A. P.; Bluhm, H.; Guo, J.; Salmeron, M. Dealloying of Cobalt from CuCo Nanoparticles under Syngas Exposure. *J. Phys. Chem. C* **2013**, *117* (12), 6259–6266.

(62) Carenco, S.; Sassoye, C.; Faustini, M.; Eloy, P.; Debecker, D. P.; Bluhm, H.; Salmeron, M. The Active State of Supported Ruthenium Oxide Nanoparticles during Carbon Dioxide Methanation. *J. Phys. Chem. C* **2016**, *120* (28), 15354–15361.

(63) Martínez-Prieto, L. M.; Carenco, S.; Wu, C. H.; Bonnefille, E.; Axnanda, S.; Liu, Z.; Fazzini, P. F.; Philippot, K.; Salmeron, M.; Chaudret, B. Organometallic Ruthenium Nanoparticles as Model Catalysts for CO Hydrogenation: A Nuclear Magnetic Resonance and Ambient-Pressure X-Ray Photoelectron Spectroscopy Study. *ACS Catal.* **2014**, *4* (9), 3160–3168.

(64) Huang, X.; Zhao, Z.; Cao, L.; Chen, Y.; Zhu, E.; Lin, Z.; Li, M.; Yan, A.; Zettl, A.; Wang, Y. M.; Duan, X.; Mueller, T.; Huang, Y. High-Performance Transition Metal-Doped Pt3Ni Octahedra for Oxygen Reduction Reaction. *Science (80-.).* **2015**, *348* (6240), 1230–1234.

(65) Cao, L.; Mueller, T. Theoretical Insights into the Effects of Oxidation and Mo-Doping on the Structure and Stability of Pt–Ni Nanoparticles. *Nano Lett.* **2016**, *16* (12), 7748–7754.

(66) Jia, Q.; Zhao, Z.; Cao, L.; Li, J.; Ghoshal, S.; Davies, V.; Stavitski, E.; Attenkofer, K.; Liu, Z.; Li, M.; Duan, X.; Mukerjee, S.; Mueller, T.; Huang, Y. Roles of Mo Surface Dopants in Enhancing the ORR Performance of Octahedral PtNi Nanoparticles. *Nano Lett.* **2018**, acs.nanolett.7b04007.

(67) Portehault, D.; Maneeratana, V.; Candolfi, C.; Deschler, N.; Veremchuk, I.; Grin, Y.; Sanchez, C.; Antonietti, M. Facile General Route toward Tunable Magneli Nanostructures and Their Use As Thermoelectric Metal Oxide/Carbon Nanocomposites. *ACS Nano* **2011**, *5*, 9052–9061.

Entry for the Table of Contents

PERSONAL ACCOUNT

Nanoalloys are a playground to establish structure-properties relationships within the nano-matter. Rational design of the synthesis parameters (oxidation state of precursors, reaction temperature, stoichiometry) gives unique access to nanoparticles with well-defined surface.

Reactivity of nanoparticles under environmental conditions is investigated. I*n situ* microscopy, near-ambient-pressure x-ray photoelectron spectroscopy and soft x-ray absorption spectroscopy highlights complex transformation of the nanoparticles under O_2, H_2 and reactive gas mixtures.

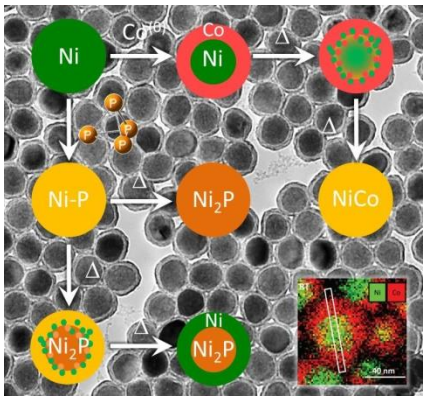

Sophie Carenco

Designing Nanoparticles and Nanoalloys with Controlled Surface and Reactivity